中国光学（中英文） Chinese Optics 核心期刊

Influence of sampling on three-dimensional surface shape measurement

QIAO Nao-sheng, Shang Xue

Citation:
QIAO Nao-sheng, Shang Xue. Influence of sampling on three-dimensional surface shape measurement[J]. *Chinese Optics*, 2024, 17(6): 1512-1520. doi: 10.37188/CO.EN-2024-0003
乔闹生, 尚雪. 抽样对三维形貌测量的影响[J]. 中国光学, 2024, 17(6): 1512-1520. doi: 10.37188/CO.EN-2024-0003

View online: https://doi.org/10.37188/CO.EN-2024-0003

文章编号 2097-1842(2024)06-1512-09

Influence of sampling on three-dimensional surface shape measurement

QIAO Nao-sheng[1,2*], Shang Xue[2]

（1. *International College*, *Hunan University of Arts and Science*, *Changde* 415000, *China*;
2. *Mathematics and Physics Science College*, *Hunan University of Arts and Science*, *Changde* 415000, *China*）

* *Corresponding author*, *E-mail*: *naoshengqiao@*163.*com*

Abstract: In order to accurately measure an object's three-dimensional surface shape, the influence of sampling on it was studied. First, on the basis of deriving spectra expressions through the Fourier transform, the generation of CCD pixels was analyzed, and its expression was given. Then, based on the discrete expression of deformation fringes obtained after sampling, its Fourier spectrum expression was derived, resulting in an infinitely repeated "spectra island" in the frequency domain. Finally, on the basis of using a low-pass filter to remove high-order harmonic components and retaining only one fundamental frequency component, the inverse Fourier transform was used to reconstruct the signal strength. A method of reducing the sampling interval, i.e., reducing the number of sampling points per fringe, was proposed to increase the ratio m between the sampling frequency and the fundamental frequency of the grating. This was done to reconstruct the object's surface shape more accurately under the condition of $m > 4$. The basic principle was verified through simulation and experiment. In the simulation, the sampling intervals were 8 pixels, 4 pixels, 2 pixels, and 1 pixel, the maximum absolute error values obtained in the last three situations were 88.80%, 38.38%, and 31.50% in the first situation, respectively, and the corresponding average absolute error values are 71.84%, 43.27%, and 32.26%. It is demonstrated that the smaller the sampling interval, the better the recovery effect. Taking the same four sampling intervals in the experiment as in the simulation can also lead to the same conclusions. The simulated and experimental results show that reducing the sampling interval can improve the accuracy of object surface shape measurement and achieve better reconstruction results.

Key words: three-dimensional surface shape measurement; sampling interval; spectra overlapping; measurement accuracy

收稿日期:2024-01-31; **修订日期**:2024-02-25

基金项目:湖南省教育厅科学研究重点项目（No. 22A0484）; 国家自然科学基金（No. 12104150）

Supported by Key Scientific Research Project of Hunan Provincial Department of Education (No. 22A0484); National Natural Science Foundation of China (No. 12104150)

抽样对三维形貌测量的影响

乔闹生[1,2*], 尚　雪[2]
（1. 湖南文理学院 国际学院, 湖南 常德 415000;
2. 湖南文理学院 数理学院, 湖南 常德 415000）

摘要: 本文研究了抽样对三维形貌测量的影响。首先, 利用傅立叶变换推出频谱表达式。在此基础上, 分析了 CCD 像元的产生过程并给出了其表达式。然后, 经抽样得到离散的变形条纹表达式, 并推导出了其傅立叶频谱表达式, 从而得到频域内无限重复的“频谱岛”。 最后, 利用低通滤波器滤除高级频谱成份后仅保留其中一个基频成份, 由逆傅立叶变换恢复信号强度。提出减小抽样间隔, 即减小每根条纹抽样点数的方法, 来增大抽样频率与光栅基频的比值 m, 使之在满足 m>4 的条件下能更准确地恢复物体的三维形貌。通过仿真和实验对基本原理进行验证。在仿真分析中, 抽样间隔分别取 8 pixels、4 pixels、2 pixels、1 pixel, 后 3 种情况所得到的最大绝对误差值分别为第一种情况下的 88.80%、38.38% 和 31.50%, 平均绝对误差值分别为第一种情况下的 71.84%、43.27% 和 32.26%。可见, 抽样间隔越小, 恢复效果越好。在实验中, 取与仿真分析相同的 4 次抽样间隔, 得到了与仿真分析相同的结论。结果表明: 减小抽样间隔可提高三维形貌的测量精度, 取得了更好的恢复效果。

关　键　词: 三维形貌测量; 抽样间隔; 频谱混叠; 测量精度
中图分类号: O438.2　　**文献标志码:** A　　**doi:** 10.37188/CO.EN-2024-0003　　**CSTR:** 32171.14.CO.EN-2024-0003

1　Introduction

Three-dimensional surface shape measurement based on grating projection is widely applied in various fields such as computer vision, physical simulation, automatic detection, biology, and medicine. It has many advantages, such as high speed, high accuracy, non-contact, automation, etc[1-3]. Many scholars around the world have researched it and have achieved good results. For example, to reduce phase measurement errors caused by measuring glossy surfaces, Zhou *et al.* proposed a pixel-by-pixel combination multi-intensity matrix projection method. It has significantly reduced the number of projection operations and time consumption[4]. Due to the influence of too many projected patterns on phase unwrapping, Yang *et al.* proposed a high-speed measurement method suitable for three-dimensional shapes which uses only three high-frequency internal shift phase modes (70 cycles), which improved measurement accuracy and speed, and obtained wrapping phase and fringe order[5]. Using the gray code method, Lu *et al.* proposed a method based on staggered gray code light, which avoided step errors without projecting additional gray code modes[6]. Due to overexposure in optical three-dimensional measurement, phase information cannot be obtained reliably. Feng *et al.* put forward a highly reflective surface measurement method based on pixel-by-pixel modulation, thereby significantly improving the measurement speed and accuracy[7].

During the measurement process, due to the fact that the CCD (Charge Coupled Device) imaging system is not a general translation invariant system but a sampling imaging system with discrete characteristics, it will cause image distortion, resulting in spectra overlapping during the transformation process, and thus bringing errors to the measurement of the three-dimensional surface shape[8-10]. Many scholars have proposed better measurement methods to reduce or eliminate these errors and improve accuracy[11-13]. Due to the nonlinear effect of CCD on high-power laser wavefront detection, Du *et al.* proposed a method to reduce or eliminate spectra overlapping caused by the CCD nonlinear effect by increasing spatial carrier frequency[11]. Due to the important role played by the nonlinearity of

scientific-level CCD in experimental processing, Cheng *et al.* used two different schemes to experimentally test the nonlinear characteristics of CCD. They achieved good experimental results[12]. Due to CCD's nonlinear effects, spectra overlapping can occur when measuring complex optical three-dimensional surface shapes. Qiao *et al.* used the dual-frequency grating projection method to eliminate the nonlinear effects of CCD and improved measurement[13].

The following sections study the influence of sampling on the measurement of three-dimensional surface shapes and provide detailed reasoning and analysis of its basic principles. They also effectively validate the basic principle analysis by conducting simulations and experiments that achieve improved results.

2 Principle analysis

Fig. 1 shows the measurement system schematic diagram. P_1P_2 is the projector's optical axis, L_0 is the distance between the optical center I_2 of the CCD imaging system and the reference plane, A and C are the points located on the reference plane, and D is the point on the object surface, h is the distance from D to the reference surface.

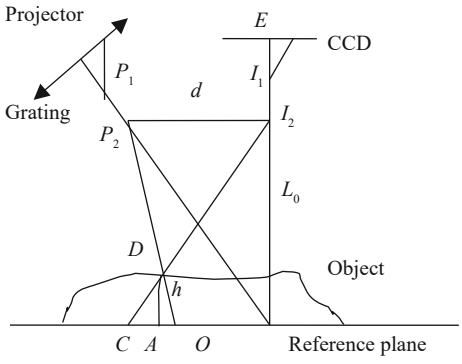

Fig. 1 Schematic diagram of the measurement system

By projecting the grating onto the surface of a three-dimensional object, the signal strength obtained by the CCD imaging system can be expressed as follows

$$g(x,y)=r(x,y)\sum_{n=-\infty}^{\infty}a_n\exp\{j[2\pi nf_0x+n\phi(x,y)]\}=\sum_{n=-\infty}^{\infty}q_n(x,y)\exp(j2\pi nf_0x)\quad,\tag{1}$$

where $r(x,y)$ is the non-uniform reflectivity of the object surface, n is the Fourier series, a_n is the n-order Fourier coefficient of $g(x,y)$, and f_0 is the fundamental frequency of grating. And $\phi(x,y)$ is the phase of the object, where $q_n(x,y)=a_nr(x,y)\exp[jn\varphi(x,y)]$.

By performing the fast Fourier transform on Eq. (1) and using π phase-shifting technology[14] to eliminate the zero-order spectra components present in the frequency domain, the spectra expression containing the object height information can be obtained as follows

$$G(f_x,f_y)=\int_{-\infty}^{\infty}\int_{-\infty}^{\infty}g(x,y)\exp[-j2\pi(f_xx+f_yy)]\mathrm{d}x\mathrm{d}y=\sum_{n=-\infty}^{\infty}Q_n(f_x-nf_0,f_y-nf_0)+\sum_{n=-\infty}^{\infty}Q_n^*(f_x-nf_0,f_y-nf_0)\quad,\tag{2}$$

where $G(f_x,f_y)$ and $Q_n(f_x,f_y)$ are the spectra obtained by Fourier transform of $g(x,y)$ and $q_n(x,y)$, respectively, and $Q_n^*(f_x,f_y)$ is the conjugate complex of $Q_n(f_x,f_y)$.

Because CCD comprises an array of several small pixels arranged neatly and tightly with a certain geometric size, each CCD has approximately hundreds of thousands or even millions of pixels[15]. Let the pixel shape be a rectangle, represented by the function $rect(x/\Delta x,y/\Delta y)$, where Δx and Δy present the pixel's dimensions in the direction of the x-axis and y-axis, respectively. Therefore, the signal strength of each pixel can be represented as the convolution of $g(x,y)$ and $rect(x/\Delta x,y/\Delta y)$, its expression is as follows

$$g'(x,y)=g(x,y)*rect\left(\frac{x}{\Delta x},\frac{y}{\Delta y}\right)\quad.\tag{3}$$

Using a comb function to sample Eq. (3), the discrete deformation fringe expression is obtained as

follows

$$g''(x,y)=g'(x,y)comb\left(\frac{x}{\Delta x_1},\frac{y}{\Delta y_1}\right)= [g(x,y)*rect\left(\frac{x}{\Delta x},\frac{y}{\Delta y}\right)]comb\left(\frac{x}{\Delta x_1},\frac{y}{\Delta y_1}\right), \quad (4)$$

where Δx_1 and Δy_1 present the sampling intervals of the fringes in the direction of the x-axis and y-axis, respectively.

The spectrum function obtained by performing Fourier transform on Eq. (4) is:

$$G''(f_x,f_y)=G(f_x,f_y)\sum_{n_x=-\infty}^{+\infty}\sum_{n_y=-\infty}^{+\infty}\delta\left(f_x-\frac{n_x}{\Delta x_1},f_y-\frac{n_y}{\Delta y_1}\right)= \frac{1}{sl}\sum_{n_x=-\infty}^{+\infty}\sum_{n_y=-\infty}^{+\infty}\mathrm{sinc}\left(\frac{n_x\pi}{s}\right)\mathrm{sinc}\left(\frac{n_y\pi}{l}\right)Q\left(f_x-f_0-\frac{n_x}{\Delta x_1},f_y-f_0-\frac{n_y}{\Delta y_1}\right), \quad (5)$$

where n_x and n_y present pixel points on the x-axis and y-axis, respectively, $s=\Delta x_1/(\Delta x+\Delta x')$ and $l=\Delta y_1/(\Delta y+\Delta y')$ present the number of sampling points for each fringe in the corresponding direction, respectively, and $\Delta x'$ and $\Delta y'$ present the pixel spacing in the corresponding direction, respectively.

Thus, the spectra of the sampling function are the infinite repetition for the spectra of the primitive continuous function in the frequency domain. This is commonly known as "spectra island"[15-19]. As a result, in addition to f_0, the higher-order spectral components, such as second and third order, are also generated.

Due to the useful information containing changes in object height within f_0 of the spectra, a suitable low-pass filter must be designed to gain the f_0 and remove the high-order spectra component.

The low-pass filter is a modulation system of a point spread function. Its filtering process is the convolution process of the spectrum function and the point spread function $G_1(f_x,f_y)$. $G_1(f_x,f_y)$ in the frequency domain is presented by a Gaussian filter as follows

$$G_1(f_x,f_y)=\frac{1}{2\pi}\exp\left(-\frac{f_x^2+f_y^2}{2\delta^2}\right), \quad (6)$$

where δ presents the standard deviation of the filter related to the degree of defocus.

The spectra signal obtained through system defocusing is

$$G'''(f_x,f_y)=G''(f_x,f_y)\otimes G_1(f_x,f_y). \quad (7)$$

By filtering, the higher-order harmonics can be well separated from f_0, so that only one of the $(1/sl)\sin c(\pi/s)\sin c(\pi/l)Q(f_x-f_0-1/\Delta x_1,f_y-f_0-1/\Delta y_1)$ is retained after filtering out the higher-order harmonic components.

Then, the inverse Fourier transform is enforced on Eq. (7) to reconstruct the signal strength taken by the CCD imaging system. The measurement system outputs the n-th sine fringe image, which is obtained by the CCD system, as shown below

$$g^{\wedge}(x,y)=F^{-1}[G'''(f_x,f_y)]= \sum_{k=-\infty}^{\infty}A_k^{\wedge}\cos\{k[2\pi f_0x+\phi(x,y)+\delta_n]\}, \quad (8)$$

where $F^{-1}[\cdot]$ presents inverse Fourier transform, $A_k^{\wedge}$ presents the Fourier coefficient of $g_n^{\wedge}(x,y)$, and δ_n presents the phase-shift amount, $\delta_n=2n\pi/n_1$, $n=1,2,\cdots,n_1$.

When the n-step phase-shift method is used, we can gain the phase as follows

$$\phi^{\wedge}(x,y)=\arctan\left[\frac{\sum_{n=1}^{N}g_n^{\wedge}(x,y)\sin(\delta_n)}{\sum_{n=1}^{N}g_n^{\wedge}(x,y)\cos(\delta_n)}\right], \quad (9)$$

where $\phi^{\wedge}(x,y)$ is the wrapped phase.

Under the conditions of the telecentric projection optical path, considering $L_o\gg h(x,y)$ in the real measurement conditions, $h(x,y)$ and $\phi^{\wedge}(x,y)$ will satisfy the relations

$$h(x,y)=-\frac{L\phi^{\wedge}(x,y)}{2\pi f_0d}. \quad (10)$$

It has been discussed in the literature [15] that in order to ensure the separation of the f_0 from other periodic spectra components and the separation of spectra components during the same period, the sampling condition $m>4$ (where $m=\Delta f/f_0$, Δf presents sampling frequency) must be satisfied. This can avoid overlapping between the f_0 and the higher-order spectra components, so as to accurately reconstruct the object shape measured. Otherwise, reconstruction is difficult.

Lastly, according to $s=\Delta x_1/(\Delta x+\Delta x')$ and $l=\Delta y_1/(\Delta y+\Delta y')$, combining the relationship $\Delta f_x=1/\Delta x_1$ as well as $\Delta f_y=1/\Delta y$ between sampling frequency and sampling interval, it can be obtained that

$$\begin{cases} m_x=\dfrac{1}{\Delta x_1 f_0}=\dfrac{1}{s(\Delta x+\Delta x')f_0} \\ m_y=\dfrac{1}{\Delta y_1 f_0}=\dfrac{1}{l(\Delta y+\Delta y')f_0} \end{cases}, \qquad (11)$$

where m_x and m_y present the sampling frequency ratio in the direction of x-axis and y-axis to f_0, respectively.

It can be seen that the method of reducing the sampling interval, i.e., the number of sampling points per fringe, to increase m, can be used to increase the accuracy of object surface shape measurements.

3 Simulation and experiment

Simulation and experiment were executed to validate the basic principle analysis.

3.1 Simulation

We performed computer simulation verification on the analysis of basic principles. Assuming that the geometric parameter of the measurement system is $L_0/d=4$. The simulated object surface shape is shown in Fig. 2 (color online), with a size of 512×512 pixels.

We projected a digital projector onto a simulated object and used a CCD camera system to obtain deformation fringes. If 40 fringes are taken, then $f_0=40/512$ fringe/pixel. Using MATLAB to process the fringes, the sampling intervals of both the x-axis and y-axis directions were 8 pixels, thus, $m=1.600\,0$ can be obtained from Eq. (11). Reducing the sampling interval of the fringes to 0.5 times the original sampling interval, i.e., the sampling interval was 4 pixels. From $s=\Delta x_1/(\Delta x+\Delta x')$ and $l=\Delta y_1/(\Delta y+\Delta y')$, it can be seen that the number of sampling points for each fringe was 0.5 times that of the original, and from Eq. (11), $m=3.200\,0$ can be obtained. It can be seen that neither of the two situations satisfied the sampling condition $m>4$. The obtained spectra diagrams are shown in Fig. 3 (a) and 3(b) (color online), respectively.

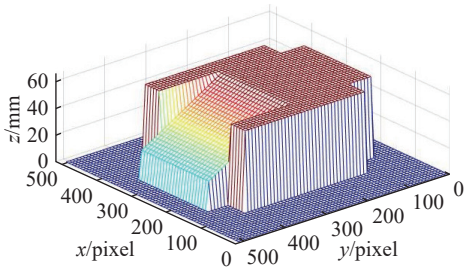

Fig. 2 The simulated object surface shape

Then, we made the sampling points of each fringe 1/4 and 1/8 times the original, i.e., the sampling interval was 2 pixels and 1 pixel, respectively. $m=6.400\,0$ and $m=12.800\,0$ can be obtained, respectively, indicating that the sampling condition $m>4$ was satisfied. The obtained spectra diagrams are shown in Fig. 3 (c) and 3(d) (color online), respectively.

In Figs. 3 (a) and 3(b), the components of f_0 in the spectra diagrams overlap with the higher-step frequency components because the sampling condition $m>4$ was not satisfied. But in Figs. 3 (c) and 3(d), the corresponding frequency components are separated because the sampling condition was satisfied. In the four sub-figures, the smaller the number of sampling points, the larger the m, and the better the separation effect.

Fig. 4 shows the surface shape errors between the reconstructed and simulated objects in the above four situations.

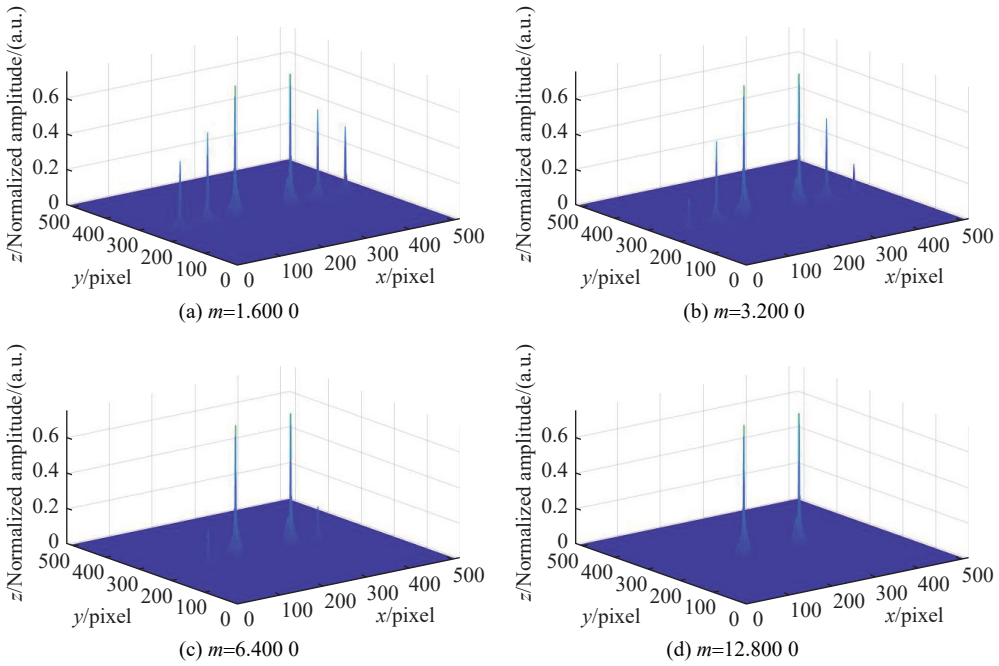

Fig. 3 The spectra diagrams

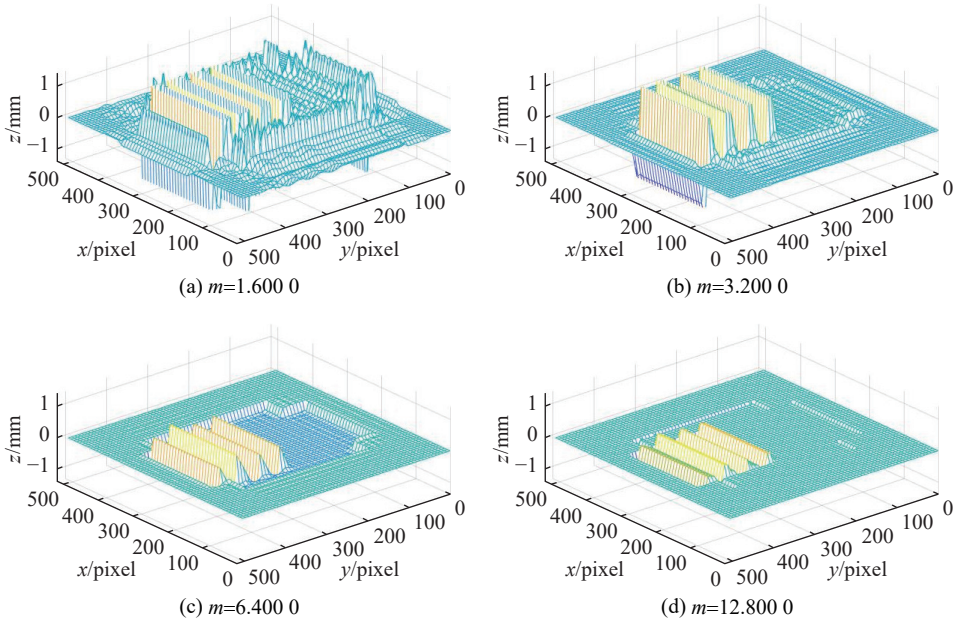

Fig. 4 The errors in the surface shape between the reconstructed and simulated objects

The maximum absolute error value (MAEV) and average absolute error value (AAEV) of each sub-image in Fig. 4 are shown in Tab. 1. The MAEV obtained from the last three sampling intervals are 88.80%, 38.38%, and 31.50%, and the AAEV are 71.84%, 43.27%, and 32.26%, respectively, of the first sampling interval.

As shown by Fig. 4 and Tab. 1, when sampling condition $m > 4$ is not satisfied, it is difficult to reconstruct the object's surface shape and has relatively large errors. On the contrary, the error is relatively small. The larger m, the smaller the error, but improving the resolution of the CCD imaging system is necessary.

Tab. 1 Error between reconstructed object and simulated object

Sampling interval	8 pixels	4 pixels	2 pixels	1 pixels
MAEV	1.3246	1.1762	0.5084	0.4173
AAEV	0.4758	0.3418	0.2059	0.1535

3.2 Experiment

To further validate the impact of CCD imaging system sampling on measuring three-dimensional surface shapes, an actual measurement experiment of a hemispherical object was carried out. As shown in Fig. 5, the simple experimental device system uses a digital projector and a low-distortion CCD camera.

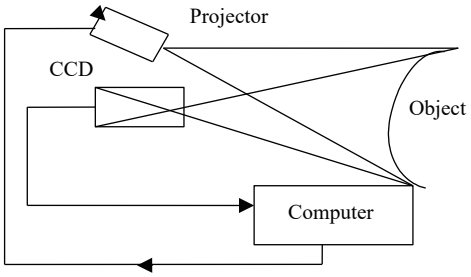

Fig. 5 The simple experimental device system

The actual experiment used the same method as the computer simulation to obtain the deformation fringes of the experimental object. 600×480 pixels and 40 fringes were taken, the fundamental frequencies were $f_x = 40/600$ fringe/pixel and $f_y = 40/480$ fringe/pixel, respectively. Using MATLAB to process the fringes, the sampling intervals of two directions were 8 pixels. From Eq. (11), $m_x = 1.875\,0$ and $m_y = 1.500\,0$ can be obtained.

Using the same method as computer simulation, the fringes' sampling interval was reduced to 0.5 times that of the original fringes, changing it to 4 pixels. Similarly, $m_x = 3.750\,0$ and $m_y = 3.000\,0$ can be obtained from Eq. (11).

Neither of the above situations satisfies the sampling condition $m > 4$. The reconstructed object surface shapes are shown in Fig. 6 (a) and 6(b) (color online).

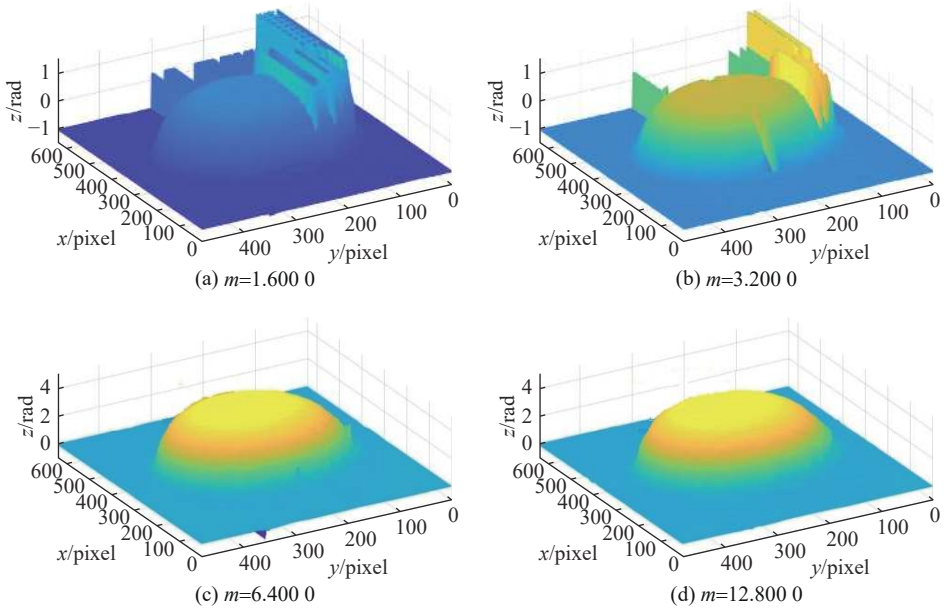

Fig. 6 Results of object surface shape reconstructed under different sampling conditions

When the sampling intervals for each fringe in the directions of the x-axis and y-axis are set to 2 pixels and 1 pixel, respectively, then $m_x = 5.625\,0$, $m_y = 4.500\,0$, and $m_x = 7.500\,0$, $m_y = 6.000\,0$ can be obtained, respectively. Both situations satisfy the sampling condition $m > 4$. The reconstructed object surface shapes are shown in Fig. 6 (c) and 6(d) (color online).

Comparing the experimental reconstruction results of the four sub-images in Fig. 6 yields the same conclusions as the computer simulation results mentioned above.

4 Conclusions

Due to the impact of sampling on the accuracy of three-dimensional surface shape measurements, the basic principles of spectra overlapping, spectra

separation, and measurement accuracy caused by sampling were analyzed and discussed.

The comb function was used to sample the signal intensity of each pixel in the CCD, and discrete deformation fringes were obtained. After the Fourier transform of the deformation fringes, the "spectra island" is generated in the frequency domain. When the method of reducing the CCD sampling interval is used, i.e., the sampling frequency is increased to satisfy the sampling condition $m > 4$, then the adjacent " spectra islands" will not overlap with the f_0; thus, reconstruction of the three-dimensional shape can be improved.

Reducing the sampling interval of pixels causes the ratio m to increase. When the sampling conditions are satisfied, the larger the m, the better the recovery of the object's three-dimensional shape. However, further improvement in the resolution of the CCD imaging system is necessary.

In the computer simulation and practical experiment, the smaller the sampling interval for each fringe, i.e., the fewer sampling points, the better the reconstruction of the object's surface shape. When sampling condition $m > 4$ is satisfied, it effectively reconstructs the object's three-dimensional shape.

References:

[1] MA X X, NI H, LU M SH, *et al*.. A measurement method for three-dimensional inner and outer surface profiles and spatial shell uniformity of laser fusion capsule[J]. *Optics & Laser Technology*, 2021, 134: 106601.

[2] FAN H, QI L, CHEN CH H, *et al*.. Underwater optical 3-D reconstruction of photometric stereo considering light refraction and attenuation[J]. *IEEE Journal of Oceanic Engineering*, 2022, 47(1): 46-58.

[3] 杨建柏, 赵建, 孙强. 基于交比不变性的投影仪标定[J]. 中国光学, 2021, 14(2): 320-328.
YANG J B, ZHAO J, SUN Q. Projector calibration based on cross ratio invariance[J]. *Chinese Optics*, 2021, 14(2): 320-328. (in Chinese).

[4] ZHOU P, WANG H Y, LAI J L, *et al*.. 3D shape measurement for shiny surface using pixel-wise composed fringe pattern based on multi-intensity matrix projection of neighborhood pixels[J]. *Optical Engineering*, 2021, 60(10): 104101.

[5] YANG SH CH, HUANG H L, WU G X, *et al*.. High-speed three-dimensional shape measurement with inner shifting-phase fringe projection profilometry[J]. *Chinese Optics Letters*, 2022, 20(11): 112601.

[6] LU L L, WU ZH J, ZHANG Q C, *et al*.. High-efficiency dynamic three-dimensional shape measurement based on misaligned gray-code light[J]. *Optics and Lasers in Engineering*, 2022, 150: 106873.

[7] 冯维, 徐仕楠, 王恒辉, 等. 逐像素调制的高反光表面三维测量方法[J]. 中国光学, 2022, 15(3): 488-497.
FENG W, XU SH N, WANG H H, *et al*.. Three-dimensional measurement method of highly reflective surface based on per-pixel modulation[J]. *Chinese Optics*, 2022, 15(3): 488-497. (in Chinese).

[8] QIAO N SH, ZHANG F. Method for reducing phase errors due to CCD nonlinearity[J]. *Optik*, 2016, 127(13): 5207-5210.

[9] LIU H Q, MA H M, TANG Q X, *et al*.. Investigation of noise amplification questions in satellite jitter detected from CCDs' parallax observation imagery: a case for 3 CCDs[J]. *Optics Communications*, 2022, 503: 127422.

[10] XUE X, ZHANG CH M, ZHAO J K, *et al*.. The influence of CCD undersampling on the encircled energy of SVOM-VT[J]. *Proceedings of the SPIE*, 2019, 11341: 1134104.

[11] 杜永兆, 冯国英, 张凯, 等. CCD 非线性效应对剪切干涉法波前检测的影响[J]. 强激光与粒子束, 2010, 22(8): 1775-1779.
DU Y ZH, FENG G Y, ZHANG K, *et al*.. Effect of CCD nonlinearity on wavefront detection by shearing interferometry[J]. *High Power Laser and Particle Beams*, 2010, 22(8): 1775-1779.

[12] 程书博, 张惠鸽, 王哲斌, 等. 科学级光学 CCD 非线性特性测试[J]. 光学学报, 2012, 32(4): 0404001.
CHENG SH B, ZHANG H G, WANG ZH B, *et al*.. Nonlinearity property testing of the scientific grade optical CCD[J]. *Acta Optica Sinica*, 2012, 32(4): 0404001. (in Chinese).

[13] 乔闹生, 孙萍. CCD 非线性效应对双频光栅三维面形测量的影响[J]. 中国光学, 2021, 14(3): 661-669.

QIAO N SH, SUN P. Influence of CCD nonlinearity effect on the three-dimensional shape measurement of dual frequency grating[J]. *Chinese Optics*, 2021, 14(3): 661-669. (in Chinese).

[14] LI J, SU X Y, GUO L R. Improved Fourier transform profilometry for the automatic measurement of three-dimensional object shapes[J]. *Optical Engineering*, 1990, 29(12): 1439-1444.

[15] QIAO N SH. Effect of CCD nonlinearity on spectrum distribution[J]. *Optik*, 2016, 127(20): 8607-8612.

[16] WANG Y, LIN B. A fast and precise three-dimensional measurement system based on multiple parallel line lasers[J]. *Chinese Physics B*, 2021, 30(2): 024201.

[17] SUN J H, ZHANG Q Y. A 3D shape measurement method for high-reflective surface based on accurate adaptive fringe projection[J]. *Optics and Lasers in Engineering*, 2022, 153: 106994.

[18] 曹智睿. 基于相移条纹投影的动态 3D 测量误差补偿技术[J]. 中国光学 (中英文), 2023, 16(1): 184-192.
CAO ZH R. Dynamic 3D measurement error compensation technology based on phase-shifting and fringe projection[J]. *Chinese Optics*, 2023, 16(1): 184-192. (in Chinese).

[19] 乔闹生, 尚雪. 非线性系统中双频光栅相位测量[J]. 中国光学 (中英文), 2023, 16(3): 726-732.
QIAO N SH, SHANG X. Phase measurement with dual-frequency grating in a nonlinear system[J]. *Chinese Optics*, 2023, 16(3): 726-732. (in Chinese).

Author Biographics:

QIAO Nao-sheng (1971—), male, born in Chaling, Hunan Province, Ph.D, Professor, International College, Hunan University of Arts and Science. His research interests are optical information processing. E-mail: naoshengqiao@163.com